
Latent Space Analysis for Melanoma Prevention

Ciro Listone

University of Naples Federico II
Naples, 80125, Italy
ciro.listone@unina.it

Aniello Murano

University of Naples Federico II
Naples, 80125, Italy
aniello.murano@unina.it

Abstract

Melanoma represents a critical health risk due to its aggressive progression and high mortality, underscoring the need for early, interpretable diagnostic tools. While deep learning has advanced in skin lesion classification, most existing models provide only binary outputs, offering limited clinical insight. This work introduces a novel approach that extends beyond classification, enabling interpretable risk modelling through a Conditional Variational Autoencoder. The proposed method learns a structured latent space that captures semantic relationships among lesions, allowing for a nuanced, continuous assessment of morphological differences. An SVM is also trained on this representation effectively differentiating between benign nevi and melanomas, demonstrating strong and consistent performance. More importantly, the learned latent space supports visual and geometric interpretation of malignancy, with the spatial proximity of a lesion to known melanomas serving as a meaningful indicator of risk. This approach bridges predictive performance with clinical applicability, fostering early detection, highlighting ambiguous cases, and enhancing trust in AI-assisted diagnosis through transparent and interpretable decision-making.

1 Introduction

Melanoma is one of the most aggressive and deadly forms of skin cancer. Despite being less common than non-melanoma skin cancers, its high metastatic potential and rapid progression make it a major clinical concern. The skin, as the largest organ of the human body, is constantly exposed to environmental and genetic risk factors that can trigger oncogenic transformations. Globally, skin cancer represents one of the most widespread malignancies [2, 3], and is typically classified into two main groups: melanoma and non-melanoma cancers. Among the non-melanoma types, basal cell carcinoma (BCC), squamous cell carcinoma (SCC), and sebaceous gland carcinoma (SGC) account for the majority of diagnoses and usually have more favorable prognoses. In contrast, melanoma, if not intercepted early, rapidly progresses to advanced stages, often leaving patients with limited therapeutic options. It is now widely acknowledged that early detection significantly improves patient survival [18], highlighting the clinical urgency of improving diagnostic tools. Traditional diagnostic methods, particularly biopsies, remain the gold standard for skin cancer detection. However, they are invasive, resource-intensive, and unsuitable for widespread screening. The proliferation of dermoscopic imaging and the rise of deep learning offer a fast, non-invasive, and scalable diagnosis.

Despite recent advances in automated skin lesion analysis, most existing approaches remain centered on binary classification (determining whether a lesion is benign or malignant) often overlooking two critical aspects for real-world clinical use: the proactive estimation of evolutionary risk in nevi and the interpretability of such assessments. While some models attempt to justify their outputs, they rarely offer insights into the underlying factors that might indicate whether a benign-appearing nevus could evolve into melanoma. In clinical settings, it is essential not just to detect malignancy, but to understand and clearly communicate the reasons for risk.

Our work bridges the aforementioned gap by introducing a novel CVAE-based approach designed not only to classify lesions, but also to estimate a continuous, interpretable measure of evolutionary risk. Unlike standard VAEs [20], CVAEs [26] incorporate class information during training, producing a latent space that is semantically structured along the benign-malignant spectrum. This informed representation enables not only accurate lesion classification but also the estimation of a continuous, interpretable risk score reflecting a lesion’s proximity to malignant patterns. To leverage the obtained latent space for diagnosis, we also train a Support Vector Machine (SVM) [9] on the learned representations. This approach achieves an average accuracy of 96.75% across five independent runs and outperformed deeper CNN-based models such as VGG19 [25], ResNet50 [15], and EfficientNetB0 [27], while also significantly reducing training time. After classification, we evaluate benign nevi’s proximity to melanoma samples in latent space by calculating the Euclidean distances to correctly classified melanomas. Nevi with distances below the 5th percentile are flagged as “suspicious,” indicating potential malignancy overlap. To refine this selection, we apply a K-nearest neighbours (KNN) [10, 14] analysis, retaining nevi surrounded by a high proportion of melanoma samples. Finally, we use latent space interpolation to visually simulate smooth transitions from benign to malignant morphology, offering an intuitive and interpretable view of disease progression. By combining diagnostic performance with geometric and visual interpretability, our approach supports transparent, proactive decision-making in clinical dermatology.

This document is structured as follows: Chapter 2 provides an overview of related work in the field. Chapter 3 describes the proposed approach in detail, including the architecture and training methodology. Chapters 4 and 5 present the experimental results and offer a discussion of the findings, respectively.

2 Related Work

Over the past two decades, convolutional neural networks (CNNs) have revolutionized medical image analysis [21], particularly for skin lesion classification [12, 18]. Transfer learning has further boosted their effectiveness by enabling pre-trained networks to be fine-tuned for dermatological tasks. Recent approaches also combine CNNs with multiscale segmentation [32] and hybrid models using pre-trained architectures [23].

While CNNs remain dominant in image classification tasks, autoencoders (AEs) have also gained attention for their ability to learn compact and meaningful representations from data. Composed of an encoder and decoder, AEs map high-dimensional data to a lower-dimensional latent space, forcing the model to retain only the most relevant features. This compression-reconstruction process is particularly effective in tasks like denoising [13], where AEs learn to remove noise and irrelevant variations. Reconstruction quality is optimized using loss functions such as Binary Cross-Entropy (BCE), Mean Squared Error (MSE), and Kullback-Leibler (KL) divergence. To overcome the limitations of basic autoencoders, such as poor generalization or lack of interpretability, various extensions have been developed. Notable variants include the Denoising Autoencoder (DAE) [30], Sparse Autoencoder (SAE) [6], Variational Autoencoder (VAE) [20], and the Conditional Variational Autoencoder (CVAE) [26], which is the focus of this work.

VAEs represent a probabilistic approach to generative modelling, introducing stochastic inference and a continuous latent space characterized by a mean " μ " and standard deviation " σ ". This enables them to approximate the underlying distribution of input data, supporting both data generation and robust feature learning. Unlike traditional AEs, VAEs adopt a probabilistic framework that makes it possible to sample from the latent space and generate new data instances. In biomedical contexts, VAEs have proven useful for learning meaningful latent representations, especially in diagnostic and prognostic settings. For example, Way and Greene [31] employed a VAE to extract biologically relevant features from RNA-seq data, facilitating tumor stratification and cancer subtype trajectory analysis. In dermatology, Lu and Xu [22] applied VAEs for anomaly detection in skin images, while Casti et al. [4] explored the sensitivity of latent representations to skin tone and imaging artifacts.

Conditional VAEs (CVAEs), an extension of VAEs (Figure 1), introduce conditional variables that guide the data generation process. By conditioning on auxiliary information, such as class labels, CVAEs enable controlled and targeted synthesis. While they retain the core architecture of VAEs, this added flexibility makes them particularly effective in applications that require fine-grained generation or class-specific modelling. Although challenges related to explainability persist, methods

like conditional latent space analysis can provide additional insight into how the model represents input data. Importantly, both VAEs and CVAEs can be integrated into image classification pipelines, leveraging their capacity to learn robust, continuous latent spaces. In classification tasks involving high-dimensional and variable data, CVAEs are especially advantageous due to their ability to associate input features with class-specific information, thereby enhancing model precision.

In this study, we chose a CVAE over a standard VAE for both empirical performance and theoretical considerations. In our experiments, latent representations derived from a standard VAE led to a Support Vector Machine classification accuracy of approximately 78%, despite good convergence of the reconstruction loss. In contrast, using latent vectors generated by a CVAE, the same classifier achieved an average accuracy of 96.75%. This substantial improvement demonstrates that incorporating conditional components enables the model to learn more structured, informative latent spaces that are highly correlated with the class labels.

To the best of our knowledge, Conditional Variational Autoencoders have not been previously applied to modelling the nevus-to-melanoma transformation, representing a novel direction investigated in this study.

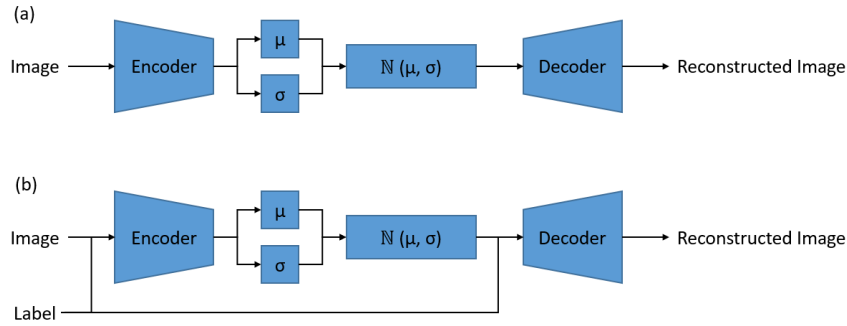


Figure 1: Typical architectures of a VAE (a) and a CVAE (b) compared

3 Methodology

3.1 Dataset and Employed Technologies

The images analysed in this paper were sourced from the public ISIC 2019 dataset [28, 7, 8], which includes eight different classes of skin lesions. However, we focused on the two most clinically relevant categories: nevi (NV) and melanomas (MEL), due to the potential for nevi to undergo malignant transformation into melanomas. This focus allowed us to fully leverage the potential of the CVAE in constructing a latent space where the distance between samples serves as an indicator of oncological risk.

To standardize the data and make it compatible with the neural network input, a preprocessing pipeline was applied. First, all images were resized to a fixed resolution of 128×128 pixels with 3 channels (RGB), regardless of their original dimensions. This ensures a consistent input size for the model while also reducing computational complexity. Subsequently, each pixel value was normalized by dividing by 255, bringing the data into the [0,1] range. This normalization step enhances the model’s learning process by improving numerical stability and accelerating convergence during training. The labels associated with the images were initially encoded as numeric values (0 for NV and 1 for MEL) and then converted to one-hot vectors, yielding binary vectors with two elements. This format is necessary for the conditional component of the CVAE model. The entire dataset was split into a training set (80%) and a test set (20%) using a stratified split to preserve the original class distribution. After this partitioning, the training set comprised 13,917 images, while the test set included 3,480 images.

The implementation was carried out using Python, with Keras [5] and TensorFlow [1] as the primary frameworks, and executed on the Kaggle platform. To optimize performance, we leveraged Kaggle’s

capability to use GPU acceleration. Specifically, we employed a high-performance NVIDIA Tesla P100 GPU, designed for deep learning applications and computationally intensive workloads.

3.2 Encoder

As previously mentioned, the Conditional Variational Autoencoder is composed of two core components: the encoder and the decoder. The encoder compresses an input image into a latent representation while preserving essential features for reconstruction or generation. Unlike a standard VAE, the CVAE conditions this process on additional semantic input, in our case the image’s class label (NV or MEL), allowing it to learn more structured and meaningful representations.

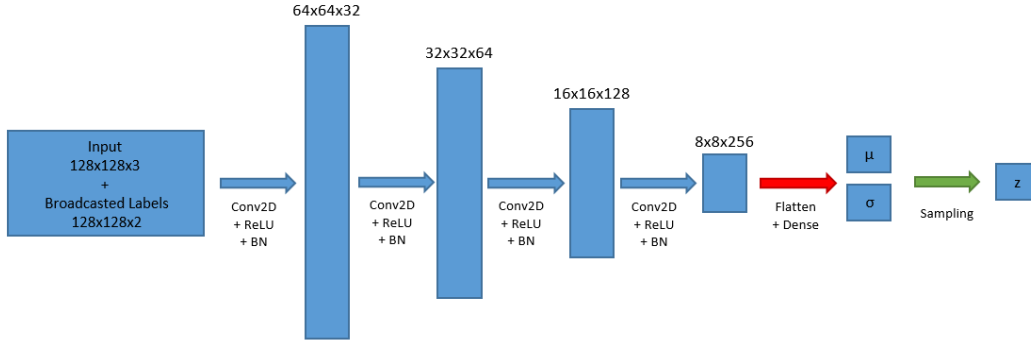


Figure 2: Encoder architecture

Specifically, our encoder (Figure 2) takes as input an RGB image and its associated one-hot encoded label. This label is broadcast across the spatial dimensions of the image, enabling the model to incorporate class information from the earliest stages of visual processing. Our encoder is built from four convolutional blocks, each consisting of a 2D convolution (3x3 kernel, stride 2), followed by a ReLU activation and a batch normalization (BN) [17], which enhances stability during training, accelerates convergence, and improves the model’s generalization. These blocks progressively reduce spatial resolution (from 128x128 to 8x8) while increasing depth (from 32 to 256 filters), capturing increasingly abstract and semantically rich features. Early layers detect local patterns like edges and textures, while deeper layers capture more complex structures. The final 8x8x256 feature map is flattened and passed through a fully connected layer with 128 units, followed by ReLU and BN. This layer consolidates the learned features into an intermediate vector, which is then projected into the latent space. In a VAE (and similarly in a CVAE), the encoder does not output a single latent vector but rather the parameters of a probability distribution, typically a multivariate Gaussian, defined by a mean (μ) and a standard deviation (σ). These parameters allow the decoder to generate diverse yet coherent samples. However, directly sampling from this distribution is non-differentiable, which would hinder training via gradient descent. To address this, the model uses the well-known reparameterization trick [20]: it samples a random variable ϵ from a normal distribution with zero mean and unit variance $\mathcal{N}(0, 1)$, and computes the latent vector as $z = \mu + \sigma \cdot \epsilon$. This reformulation expresses the sampling operation as a differentiable function of μ and σ , enabling backpropagation. This mechanism allows the model to learn a latent space aligned with the data by optimizing a loss function that combines two terms: the reconstruction error and the Kullback-Leibler divergence between the learned distribution and the standard normal prior. Through the reparameterization trick, the model retains both generative power and efficient optimization.

Ultimately, the encoder outputs a latent sample derived from the learned mean and standard deviation. This sample is then passed to the decoder, which generates new images. The stochastic nature of this sampling introduces controlled variability, allowing the model to produce diverse yet class-consistent outputs.

3.3 Decoder

In the context of a CVAE, the decoder is responsible for reconstructing an image from a latent representation, while taking into account the provided condition (e.g., a class label). In other words, the decoder generates synthetic data that aligns with a learned distribution, constrained by the desired label.

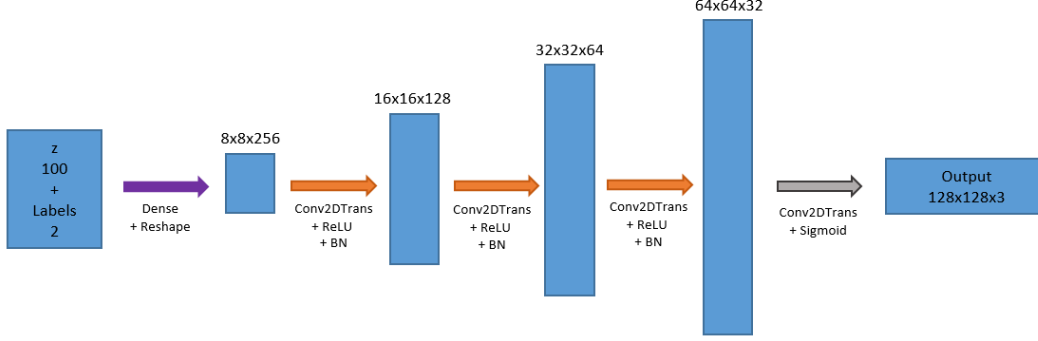


Figure 3: Decoder architecture

The decoder (Figure 3) receives as input a latent vector, sampled according to the distribution learned by the encoder, and combines it with the class label. This concatenation ensures that class-related information is incorporated from the very beginning of the generative process, allowing the decoder to guide image generation in a way that is consistent with the specified class. Theoretically, this operation allows the latent variable to be treated not as an isolated entity but as a conditioned vector, enabling explicit control over the characteristics of the generated data. After concatenation, the resulting vector is transformed through a dense layer into a high-dimensional representation, which is then reshaped into a three-dimensional tensor. The operations performed by our decoder reverse the compression process carried out by the encoder: starting from a compact representation a spatially-structured data format suitable for image interpretation is progressively reconstructed. This initial phase provides a structural basis upon which subsequent convolutional layers operate to generate the final image. The image is generated through a sequence of transposed convolutions, which function symmetrically to the convolutional layers in the encoder. Each transposed layer gradually increases the spatial resolution of the activation map, expanding it until it reaches the original dimensions of the input image. At each step, spatial upsampling is performed (using stride = 2), increasing the height and width, while the tensor's depth decreases, guiding the transition from abstract internal representations to interpretable visual structures. ReLU is then applied after each convolution, introducing non-linearity into the transformation process and enabling the model to learn more complex representations. As in the encoder, each convolutional block is followed by a batch normalization operation. This is particularly important in the decoder, where the generative process can easily degenerate into incoherent solutions if not properly regularized.

The final layer of the decoder produces a synthetic image with the same number of channels as the input image (3 for RGB images). The final activation is a sigmoid function, which compresses the output values into the range $[0,1]$, in line with the normalization applied to the original image.

3.4 Training and Evaluation

In a CVAE, the loss function is a crucial component that combines two terms: the reconstruction error and the KL divergence. The first term is computed using the Mean Squared Error between the original image and the one reconstructed by the decoder. The MSE quantifies how much the generated images deviate from the originals, penalizing pixel-wise differences. The KL divergence, on the other hand, measures the difference between the learned latent distribution and the standard normal distribution (with zero mean and unit variance). It is calculated using the mean and standard deviation parameters produced by the encoder. This term serves to regularize the latent space, preventing the learned

distribution from diverging too far from the desired one. The total loss function is the sum of the reconstruction error and the KL divergence. The CVAE was trained on the initial training set, with 20% of the data reserved as a validation set. This approach facilitates monitoring the loss trend and helps prevent overfitting, ensuring the generative model correctly maps images and labels into the latent space while maintaining generalization capabilities. The optimization process during CVAE training was handled using the Adam optimizer [19], a popular choice in neural networks due to its adaptive learning rates. Adam combines the advantages of momentum and Adagrad, providing a more stable and faster gradient descent. It is particularly effective for complex models like the CVAE, enabling efficient parameter updates even with noisy data and intricate gradients.

Once the CVAE was trained, the latent representations (i.e., latent vectors) were extracted from the encoder and scaled, to be subsequently used as input for an SVM classifier. The performance of the SVM was evaluated using the initial test set (representing 20% of the original data not used in training). The evaluated metrics include accuracy, precision, recall, F1-score, and ROC AUC, providing a comprehensive measure of the model's ability to correctly distinguish between the NV and MEL classes based on the latent representations learned by the CVAE. This process makes it possible to assess how effectively the information learned by the generative model can be leveraged for classification tasks, exploiting the compact and informative representation of the latent space.

3.5 Risk Analysis

After performing the prediction with the SVM on the test set, a distance-based analysis is conducted to evaluate the similarity of benign nevi with respect to melanoma samples in the latent space. For each correctly classified nevus, the Euclidean distances to all correctly classified melanomas are computed using both the minimum and average distances. This allows for quantifying how closely each benign sample is positioned relative to the melanoma representations in the learned latent space. To automatically identify potentially suspicious nevi, threshold values are defined based on the 5th percentile of the overall distributions of minimum and average distances. Nevi falling below either threshold are flagged as "suspicious", as their proximity to the melanoma representations suggests a possible overlap in latent characteristics typically associated with malignancy. To further refine the identification of suspicious nevi, a KNN analysis is applied to the previously selected candidates. For each nevus, the number of melanoma samples among its K nearest neighbours in the latent space is computed. Nevi surrounded by a number of melanomas exceeding a certain threshold, arbitrarily chosen, are retained as final high-risk candidates. This additional filtering step combines global similarity with local neighbourhood structure, enhancing the robustness of the risk assessment.

This entire process refines the classification of nevi by integrating SVM predictions with proximity-based and distance-based analyses in the latent space. Such an approach offers a robust model for identifying potentially at-risk nevi, which could support physicians in making more accurate and timely diagnostic decisions.

4 Results

This chapter presents the quantitative results obtained from the CVAE model and discusses their implications. The reported metrics represent the average of five independent runs, in order to reduce the influence of random splits into training, validation, and test sets on the final values. In each run, the CVAE was trained for 20 epochs, achieving an average validation loss of approximately 0.1324. Memory usage on the GPU started at 19.03 MB before training and increased to 57.83 MB after training. The machine had a total of 33.66 GB of RAM, with memory usage rising from 11.75 GB to 13.11 GB following the training. These resource measurements suggest that the model made moderate use of the available GPU memory and RAM throughout the training process.

Since a SVM classifier was used to evaluate the quality of the latent representations produced by the encoder, standard classification metrics such as accuracy, precision, recall, F1-score, and ROC AUC can be employed. These metrics showed high values across all runs, indicating that the latent vectors contain effective discriminative information. On average, the model achieved an accuracy of 96.75%, a precision of 94.43%, a recall of 93.02%, an F1-score of 93.72%, and an average ROC AUC of 0.991 demonstrating not only the model's effectiveness in encoding diagnostic information but also its consistency across different random splits of the dataset. Variations between runs were limited, indicating good performance stability.

Table 1: Classification metrics for each test run

Test	Accuracy	Precision	Recall	F1-score	ROC AUC
Test 1	98.70%	97.77%	97.24%	97.53%	0.998
Test 2	97.12%	95.17%	93.70%	94.48%	0.993
Test 3	95.83%	93.18%	90.61%	91.88%	0.988
Test 4	96.98%	94.94%	93.37%	94.15%	0.992
Test 5	95.11%	91.07%	90.17%	90.57%	0.984
Average \pm Std	96.75% \pm 1.23%	94.43% \pm 2.23%	93.02% \pm 2.54%	93.72% \pm 2.39%	0.991 \pm 0.005

To contextualize these results, we compared the proposed CVAE-based approach with a series of standard convolutional neural networks, both trained from scratch and fine-tuned with ImageNet [11] pretrained weights. Each model was trained on the same dataset for 20 epochs and their performance was evaluated on the same held-out test set. The goal of this comparison was to assess not only classification performance, but also computational efficiency and robustness. As shown in Table 2, the CVAE, coupled with SVM classifier on its latent vectors, consistently outperformed all baseline CNN models achieving higher accuracy, precision, recall, and ROC AUC values, while requiring significantly less training time. These findings underscore the effectiveness of the CVAE in extracting compact and discriminative features for classification tasks.

Table 2: Comparison of classification performance and training time across models

Model	Accuracy	Precision	Recall	F1-score	ROC AUC	Training Time (s)
CVAE + SVM	98.05%	96.14%	96.35%	96.24%	0.9984	127.58
VGG19 [25]	80.29%	62.81%	59.34%	61.02%	0.8348	804.36
EfficientNetB0 [27]	78.56%	64.12%	39.89%	49.18%	0.7953	467.19
ResNet50 [15]	78.88%	62.07%	48.29%	54.32%	0.7980	631.32
VGG19 (Imagenet)	86.28%	80.06%	63.43%	70.78%	0.8952	827.93
EfficientNetB0 (Imagenet)	86.61%	75.09%	72.60%	73.82%	0.9129	504.64
ResNet50 (Imagenet)	83.56%	68.77%	67.40%	68.08%	0.8763	638.84

To analyze the latent space learned by the CVAE, three dimensionality reduction techniques, PCA [16], t-SNE [29], and UMAP [24], were applied to project the 100-dimensional latent vectors into 2D. While this reduction inevitably introduces some information loss, it facilitates the visual and quantitative assessment of latent structure. PCA, being a linear method, produced weakly grouped representations (Silhouette: 0.139, Calinski-Harabasz: 72.77, Davies-Bouldin: 6.13). Non-linear methods performed better overall: t-SNE yielded higher Calinski-Harabasz (266.92) and lower Davies-Bouldin (2.87) scores, although its Silhouette score (0.085) was the lowest, suggesting close or overlapping groups. UMAP showed more balanced results (Silhouette: 0.124, Calinski-Harabasz: 243.73, Davies-Bouldin: 2.91), indicating a favourable trade-off between local and global structure. For reference, metrics in the original 100D latent space were slightly superior (Silhouette: 0.121, Calinski-Harabasz: 294.93, Davies-Bouldin: 2.61), consistent with the expectation that the full latent space better preserves the underlying structure. Nonetheless, the relatively small differences confirm that the 2D projections still capture the main structural patterns of the latent space.

Notably, even in the original latent space, the separation between NV and MEL classes is not perfect, suggesting a degree of morphological continuity in the input data. This observation does not indicate a limitation of the model, but rather reflects the CVAE’s ability to capture subtle and complex shared patterns between classes that likely correspond to clinically ambiguous or borderline cases. The overlap in the latent space may therefore encode diagnostically relevant uncertainty, identifying nevi that share latent traits with melanomas and thus requiring closer examination. To explore this hypothesis, an interpolation analysis was conducted between selected suspicious nevi (identified based on their proximity to melanoma samples in the latent space) and their nearest melanoma counterparts. Logistic interpolations were computed in the latent space and decoded into image sequences, simulating a plausible morphological trajectory from benign to malignant features (Figure 4). While these sequences do not represent actual clinical evolution, they offer a coherent

visualization of the feature transitions that the model considers most significant for distinguishing between the two classes. The interpolated images display smooth, structured transformations, supporting the interpretation of the latent space as continuous and semantically meaningful. These visualizations can serve as valuable tools for illustrating potential diagnostic pathways and for identifying lesions that fall within zones of diagnostic ambiguity, thus enhancing the interpretability and clinical relevance of the proposed model.

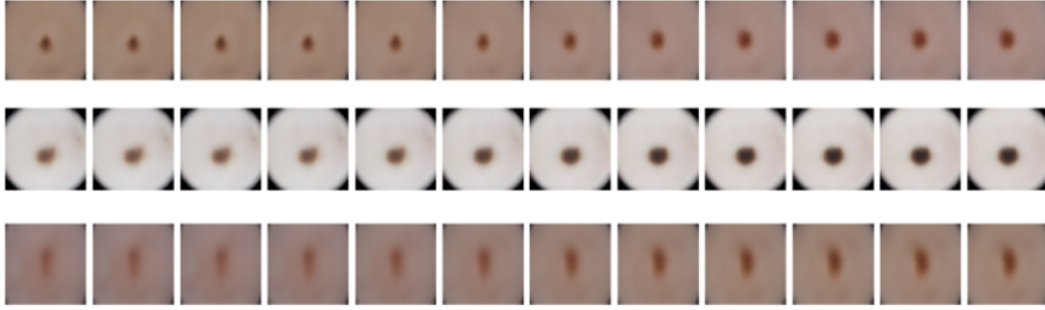


Figure 4: Examples of interpolation between a nevus (far left) and a melanoma (far right) based on CVAE reconstructions

In contrast to the previously reported metrics, the analysis of distances between nevi and melanomas does not yield consistent average values across different model runs. This instability is primarily due to randomness in data splitting and the inherent stochasticity of model training. Notably, the indices of the closest nevi can significantly vary across runs. This high variability makes it difficult to draw robust, reproducible conclusions based on individual pairwise comparisons in the latent space. For this reason, instead of presenting average results, a representative example was chosen to illustrate the process. During the analysis, as mentioned in Chapter 3, a preliminary filtering step was applied to identify nevi with significant structural proximity to melanomas. In particular, two types of distances were computed between nevi and melanomas in the latent space: the average distance and the minimum distance. Nevi showing a distance below the 5th percentile for either of these metrics were selected as potentially suspicious. The KNN analysis was then performed to refine this filtering further and reduce the risk of false positives. This phase aimed to identify nevi that were potentially suspicious based on their proximity to melanomas in the latent space. For each nevus, the 10 nearest neighbours were retrieved, and the number of melanomas among them was counted. Nevi with at least 4 melanomas in their neighbourhood were classified as suspicious (Table 3).

In the representative case, one suspicious nevus had 7 melanomas among its 10 closest neighbours, indicating a strong structural similarity to melanomas. Other nevi displayed similar results, with 6 melanomas among their nearest neighbours, confirming their critical position in the latent space.

5 Conclusion

This work introduces a novel application of Conditional Variational Autoencoders in the classification of melanoma and nevi, supporting more accurate and interpretable diagnosis. Unlike traditional methods that typically focus solely on classification, our method leverages the power of CVAEs to generate latent representations that capture the complex, underlying structure of skin lesions. These representations not only allow for a highly accurate distinction between benign nevi and melanomas, but also provide a deeper, interpretable understanding of lesion characteristics that can be directly utilized to support clinical decision-making. This interpretability is particularly crucial when dealing with lesions that present borderline features or ambiguous characteristics, as the model is specifically designed to uncover subtle morphological variations that might otherwise be missed by standard diagnostic pipelines.

A key scientific contribution of this work is the innovative use of latent space analysis to identify nevi that may be at risk of progressing to melanoma. By evaluating the proximity of benign nevi to

Table 3: Suspicious nevi with at least 4 melanomas among the 10 nearest neighbours in the latent space

Nevus ID	mean_dist	min_dist	near_mels
Nevus 1	12.624	3.791	7
Nevus 2	13.057	4.916	6
Nevus 3	12.570	4.108	6
Nevus 4	13.092	4.306	5
Nevus 5	13.059	5.310	5
Nevus 6	12.693	4.936	5
Nevus 7	12.997	5.157	4
Nevus 8	13.151	4.991	4
Nevus 9	12.224	3.997	4
Nevus 10	12.673	4.669	4
Nevus 11	13.077	4.706	4
Nevus 12	13.138	4.350	4
Nevus 13	12.845	4.896	4
Nevus 14	12.695	5.289	4
Nevus 15	12.565	4.071	4
Nevus 16	12.597	5.182	4
Nevus 17	13.222	5.205	4
Nevus 18	13.879	5.118	4
Nevus 19	12.939	4.134	4

melanoma representations within the learned latent space, our model uncovers continuous patterns of dermatological risk that reflect the gradual evolution from benign to malignant features. This enables the early identification of suspicious lesions even before clinical signs of malignancy are evident. Specifically, the model analyses indicators such as the average or minimum distance of a nevus to melanoma embeddings and examines the local composition of nearest neighbours in latent space. These complementary tools provide a systematic and objective approach for flagging potentially high-risk lesions, offering clinicians additional means of surveillance and risk stratification even in the absence of overt malignancy.

In terms of performance, the results demonstrate that our approach is highly effective in accurately classifying skin lesions, with a level of robustness and consistency that surpasses the considered baseline models. The combination of a CVAE and a Support Vector Machine classifier has shown to produce semantically meaningful latent representations that ensure high accuracy in distinguishing between benign and malignant cases. This dual nature of the model, being both predictive and exploratory, makes it particularly suitable for clinical contexts where the goal is not only to classify but also to monitor, explain, and inform diagnostic decisions.

Beyond performance metrics, the model introduces a crucial element of interpretability by offering a geometric and patient-specific perspective on skin lesion data. Through navigation and interpolation in the latent space, clinicians can simulate transitions between benign and malignant phenotypes, creating visual narratives that explain uncertainty and illustrate possible evolutionary trajectories. This communicative capacity adds significant value in shared decision-making scenarios, where conveying risk in an accessible yet evidence-based manner is critical. When properly calibrated, the CVAE architecture enriches the diagnostic workflow, aligning cutting-edge AI with the nuanced demands of clinical dermatology.

Nonetheless, the model’s reliance on preprocessed images captured in controlled settings and the lack of dermatologist validation limits its generalizability in real-world clinical contexts. It should be noted that some decisions, such as the use of distance thresholds and KNN, rely on logical heuristics rather than clinical validation. Integrating medical expertise in these choices will further enhance the model’s accuracy and clinical applicability. In doing so, this approach contributes to the development of AI-driven tools that combine deep generative models with the clinical rigor necessary for meaningful adoption.

References

- [1] Martín Abadi, Ashish Agarwal, Paul Barham, Eugene Brevdo, Zhifeng Chen, Craig Citro, Greg S. Corrado, Andy Davis, Jeffrey Dean, Matthieu Devin, Sanjay Ghemawat, Ian Goodfellow, Andrew Harp, Geoffrey Irving, Michael Isard, Yangqing Jia, Rafal Jozefowicz, Lukasz Kaiser, Manjunath Kudlur, Josh Levenberg, Dandelion Mané, Rajat Monga, Sherry Moore, Derek Murray, Chris Olah, Mike Schuster, Jonathon Shlens, Benoit Steiner, Ilya Sutskever, Kunal Talwar, Paul Tucker, Vincent Vanhoucke, Vijay Vasudevan, Fernanda Viégas, Oriol Vinyals, Pete Warden, Martin Wattenberg, Martin Wicke, Yuan Yu, and Xiaoqiang Zheng. TensorFlow: Large-scale machine learning on heterogeneous systems, 2015. Software available from tensorflow.org.
- [2] Rehan Ashraf, Sitara Afzal, Attiq Ur Rehman, Sarah Gul, Junaid Baber, Maheen Bakhtyar, Irfan Mehmood, Oh-Young Song, and Muazzam Maqsood. Region-of-interest based transfer learning assisted framework for skin cancer detection. *IEEE Access*, 8:147858–147871, 2020.
- [3] Allyson L Byrd, Yasmine Belkaid, and Julia A Segre. The human skin microbiome. *Nature Reviews Microbiology*, 16(3):143–155, 2018.
- [4] Paola Casti, Arianna Mencattini, Sara Cardarelli, Gianni Antonelli, Joanna Filippi, Michele D’Orazio, and Eugenio Martinelli. Sensitivity analysis of latent variables in variational autoencoders for dermoscopic image analysis. In *2022 IEEE International Symposium on Medical Measurements and Applications (MeMeA)*, pages 1–6. IEEE, 2022.
- [5] Francois Chollet et al. Keras, 2015.
- [6] Adam Coates, Andrew Ng, and Honglak Lee. An analysis of single-layer networks in unsupervised feature learning. In *Proceedings of the fourteenth international conference on artificial intelligence and statistics*, pages 215–223. JMLR Workshop and Conference Proceedings, 2011.
- [7] Noel CF Codella, David Gutman, M Emre Celebi, Brian Helba, Michael A Marchetti, Stephen W Dusza, Aadi Kalloo, Konstantinos Liopyris, Nabin Mishra, Harald Kittler, et al. Skin lesion analysis toward melanoma detection: A challenge at the 2017 international symposium on biomedical imaging (isbi), hosted by the international skin imaging collaboration (isic). In *2018 IEEE 15th international symposium on biomedical imaging (ISBI 2018)*, pages 168–172. IEEE, 2018.
- [8] Marc Combalia, Noel CF Codella, Veronica Rotemberg, Brian Helba, Veronica Vilaplana, Ofer Reiter, Cristina Carrera, Alicia Barreiro, Allan C Halpern, Susana Puig, et al. Bcn20000: Dermoscopic lesions in the wild. *arXiv preprint arXiv:1908.02288*, 2019.
- [9] Corinna Cortes and Vladimir Vapnik. Support-vector networks. *Machine learning*, 20:273–297, 1995.
- [10] Thomas Cover and Peter Hart. Nearest neighbor pattern classification. *IEEE transactions on information theory*, 13(1):21–27, 1967.
- [11] Jia Deng, Wei Dong, Richard Socher, Li-Jia Li, Kai Li, and Li Fei-Fei. Imagenet: A large-scale hierarchical image database. In *2009 IEEE conference on computer vision and pattern recognition*, pages 248–255. Ieee, 2009.
- [12] Mahmoud Elgamal. Automatic skin cancer images classification. *International Journal of Advanced Computer Science and Applications*, 4(3), 2013.
- [13] Gökçen Eraslan, Lukas M Simon, Maria Mircea, Nikola S Mueller, and Fabian J Theis. Single-cell rna-seq denoising using a deep count autoencoder. *Nature communications*, 10(1):390, 2019.
- [14] Gongde Guo, Hui Wang, David Bell, Yaxin Bi, and Kieran Greer. Knn model-based approach in classification. In *On The Move to Meaningful Internet Systems 2003: CoopIS, DOA, and ODBASE: OTM Confederated International Conferences, CoopIS, DOA, and ODBASE 2003, Catania, Sicily, Italy, November 3-7, 2003. Proceedings*, pages 986–996. Springer, 2003.

- [15] Kaiming He, Xiangyu Zhang, Shaoqing Ren, and Jian Sun. Deep residual learning for image recognition. In *Proceedings of the IEEE conference on computer vision and pattern recognition*, pages 770–778, 2016.
- [16] Harold Hotelling. Analysis of a complex of statistical variables into principal components. *Journal of educational psychology*, 24(6):417, 1933.
- [17] Sergey Ioffe and Christian Szegedy. Batch normalization: Accelerating deep network training by reducing internal covariate shift. In *International conference on machine learning*, pages 448–456. pmlr, 2015.
- [18] Muhammad Qasim Khan, Ayyaz Hussain, Saeed Ur Rehman, Umair Khan, Muazzam Maqsood, Kashif Mehmood, and Muazzam A Khan. Classification of melanoma and nevus in digital images for diagnosis of skin cancer. *IEEE Access*, 7:90132–90144, 2019.
- [19] Diederik P Kingma and Jimmy Ba. Adam: A method for stochastic optimization. *arXiv preprint arXiv:1412.6980*, 2014.
- [20] Diederik P Kingma, Max Welling, et al. Auto-encoding variational bayes, 2013.
- [21] Yann LeCun, Bernhard Boser, John S Denker, Donnie Henderson, Richard E Howard, Wayne Hubbard, and Lawrence D Jackel. Backpropagation applied to handwritten zip code recognition. *Neural computation*, 1(4):541–551, 1989.
- [22] Yuchen Lu and Peng Xu. Anomaly detection for skin disease images using variational autoencoder. *arXiv preprint arXiv:1807.01349*, 2018.
- [23] Amirreza Mahbod, Gerald Schaefer, Chunliang Wang, Rupert Ecker, and Isabella Ellinge. Skin lesion classification using hybrid deep neural networks. In *ICASSP 2019-2019 IEEE international conference on acoustics, speech and signal processing (ICASSP)*, pages 1229–1233. IEEE, 2019.
- [24] Leland McInnes, John Healy, and James Melville. Umap: Uniform manifold approximation and projection for dimension reduction. *arXiv preprint arXiv:1802.03426*, 2018.
- [25] Karen Simonyan and Andrew Zisserman. Very deep convolutional networks for large-scale image recognition. *arXiv preprint arXiv:1409.1556*, 2014.
- [26] Kihyuk Sohn, Honglak Lee, and Xinchen Yan. Learning structured output representation using deep conditional generative models. *Advances in neural information processing systems*, 28, 2015.
- [27] Mingxing Tan and Quoc Le. Efficientnet: Rethinking model scaling for convolutional neural networks. In *International conference on machine learning*, pages 6105–6114. PMLR, 2019.
- [28] Philipp Tschandl, Cliff Rosendahl, and Harald Kittler. The ham10000 dataset, a large collection of multi-source dermatoscopic images of common pigmented skin lesions. *Scientific data*, 5(1):1–9, 2018.
- [29] Laurens Van der Maaten and Geoffrey Hinton. Visualizing data using t-sne. *Journal of machine learning research*, 9(11), 2008.
- [30] Pascal Vincent, Hugo Larochelle, Yoshua Bengio, and Pierre-Antoine Manzagol. Extracting and composing robust features with denoising autoencoders. In *Proceedings of the 25th international conference on Machine learning*, pages 1096–1103, 2008.
- [31] Gregory P Way and Casey S Greene. Extracting a biologically relevant latent space from cancer transcriptomes with variational autoencoders. In *PACIFIC SYMPOSIUM on BIOCOMPUTING 2018: Proceedings of the Pacific Symposium*, pages 80–91. World Scientific, 2018.
- [32] Lequan Yu, Hao Chen, Qi Dou, Jing Qin, and Pheng-Ann Heng. Automated melanoma recognition in dermoscopy images via very deep residual networks. *IEEE transactions on medical imaging*, 36(4):994–1004, 2016.